

Can a protophobic vector boson explain the ATOMKI anomaly?

Xilin Zhang^{1,*} and Gerald A. Miller^{2,†}

¹Department of Physics, The Ohio State University, Ohio 43210, USA

²Department of Physics, University of Washington, Seattle, WA 98195, USA

(Dated: June 12, 2022)

In 2016, the ATOMKI collaboration announced [PRL **116**, 042501 (2016)] observing an unexpected enhancement of the e^+e^- pair production signal in one of the ^8Be nuclear transitions induced by an incident proton beam on a ^7Li target. Many beyond-standard-model physics explanations have subsequently been proposed. One popular theory is that the anomaly is caused by the creation of a protophobic vector boson (X) with a mass around 17 MeV [e.g., PRL **117**, 071803 (2016)] in the nuclear transition. We study this hypothesis by deriving an isospin relation between photon and X couplings to nucleons. This allows us to find simple relations between protophobic X -production cross sections and those for measured photon production. The net result is that X production is dominated by a direct $E1^X$ transition without going through any nuclear resonance (*i.e.* Bremsstrahlung radiation) with a smooth energy dependence that occurs for all proton beam energies above threshold. This contradicts the experimental observations and invalidates the protophobic vector boson explanation.

Ref. [1] announced finding of an anomaly in measuring e^+e^- pair production in ^8Be 's nuclear transition between one of its 1^+ resonances and its 0^+ ground state. Fig. 1 shows the relevant energy levels [2]. The two 1^+ resonances are barely above the $^7\text{Li} + p$ threshold; the higher-energy resonance is mostly isoscalar (MIS) while the other one is mostly isovector (MIV).] The unexpected enhancement of the signal was observed in the large e^+e^- invariant mass region (about 17 MeV) and in the large pair-correlation angles (near 140°) region. This observation has generated many beyond-standard-model physics proposals to explain this ATOMKI anomaly (*e.g.*, [1, 3, 4]).

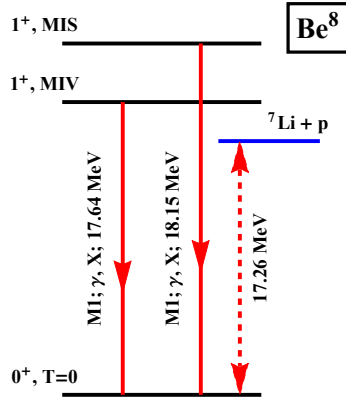


FIG. 1. The ^8Be levels [2] that are relevant for the M1 transitions producing photon (γ) and recently proposed vector boson X [3, 5, 6]. The two 1^+ resonance states are either mostly isovector (MIV) or mostly isoscalar (MIS). The blue line is the $^7\text{Li} + p$ threshold. Note X and (off-shell) γ can further decay into e^+e^- .

Our focus here is on the protophobic vector boson explanation (see *e.g.* [3, 5, 6]). The physics of a boson that almost does not interact with protons provides an interesting contrast with photon-nucleon interactions. The photon-quark interactions are given by the corresponding electromagnetic (EM) current

$$j_\gamma^\mu = \bar{Q}\gamma^\mu \left(\frac{1}{6} + \frac{\tau_3}{2} \right) Q, \quad (1)$$

where Q is the iso-doublet quark field ($Q = (u, d)^T$) and τ_3 the isospin operator. The term containing τ_3 is said to be isovector j_v^μ and the other term isoscalar j_s^μ . This leads to the nucleon-level currents:

$$J_\gamma^\mu = \bar{N} \left[\left(\frac{1}{2}\gamma^\mu + \lambda^{(0)} \frac{\sigma^{\mu\nu} i q_\nu}{2M_N} \right) + \left(\frac{1}{2}\gamma^\mu + \lambda^{(1)} \frac{\sigma^{\mu\nu} i q_\nu}{2M_N} \right) \tau_3 \right] N, \quad (2)$$

with $N = (p, n)^T$, $\lambda^{(0)} = -0.06$ and $\lambda^{(1)} = 1.85$. These give the proton magnetic moment as $\mu_p = 1 + \lambda^{(0)} + \lambda^{(1)} = 2.79$ and $\mu_n = \lambda^{(0)} - \lambda^{(1)} = -1.91$. The ratio $\mu_n/\mu_p = -0.684$, in excellent agreement with the non-relativistic quark-model result of $-2/3$ [7]. Again the term containing τ_3 is said to be isovector J_v^μ and the other term isoscalar J_s^μ .

The general form of the coupling of a new vector boson (X) to quarks is given by using [5, 6]

$$j_X^\mu = \bar{Q}\gamma^\mu \left(\frac{\varepsilon_s}{6} - \frac{\varepsilon_v \tau_3}{2} \right) Q, \quad (3)$$

where ε_s and $(-\varepsilon_v)$ are the ratios between the X and γ coupling constants in the isoscalar and isovector components. When $\varepsilon_s \approx \varepsilon_v$, X is considered to be protophobic, because the X -proton charge-coupling would be much smaller than the X -neutron one.

Comparing Eq. (1) with Eq. (3) is instructive. First note that following Eq. (3) with $\varepsilon_s = \varepsilon_v$ the X - p charge

* zhang.10038@osu.edu

† miller@phys.washington.edu

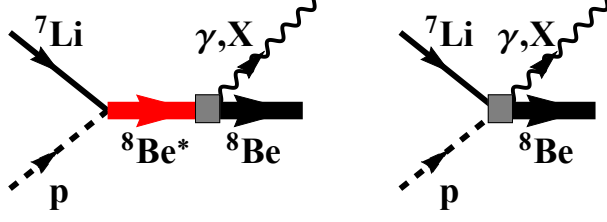


FIG. 2. The Feynman diagrams for the $M1$ and $M1^X$ (left), and $E1$ and $E1^X$ (right) transitions. In the left diagram, the intermediate ${}^8\text{Be}^*$ states are the two 1^+ resonances.

coupling vanishes because there are two u and one d valence quarks in proton, but X - n charge coupling is ε_v times that of γ - p . The X -coupling and EM currents are related by an isospin rotation, $P_y(\pi)$, of 180° about the y -axis in isospin space that changes τ_3 into $-\tau_3$. More formally, we write the isospin relation as

$$j_X^\mu = P_y(\pi) (\varepsilon_s j_s^\mu + \varepsilon_v j_v^\mu) P_y^\dagger(\pi). \quad (4)$$

This relation tells us that, after accounting for kinematic effects (for boson momentum q^μ , $q_\mu q^\mu = M_X^2$ for X and 0 for γ) of the non-zero mass of the X boson, and the different polarization vectors, the *isovector* components in the X - and γ -generating transition matrix elements are related by a simple factor of $-\varepsilon_v$. The isovector component dominates over the isoscalar one in all of the relevant transitions, see below. The resulting nucleon-level current, obtained by the isospin rotation is given by

$$J_X^\mu = \bar{N} \left[\varepsilon_s \left(\frac{1}{2} \gamma^\mu + \lambda^{(0)} \frac{\sigma^{\mu\nu} i q_\nu}{2M_N} \right) - \varepsilon_v \left(\frac{1}{2} \gamma^\mu + \lambda^{(1)} \frac{\sigma^{\mu\nu} i q_\nu}{2M_N} \right) \tau_3 \right] N. \quad (5)$$

This means that while the Dirac (γ^μ) coupling of the X to nucleons is protophobic, the Pauli ($\sigma^{\mu\nu}$) coupling cannot be so. Furthermore, in the non-relativistic quark model the ratio of neutron to proton X -magnetic moments is $-3/2$ if $\varepsilon_s = \varepsilon_v$.

The next step is to apply the existing understanding of the EM transitions in ${}^8\text{Be}$ [2, 8, 9]. The special feature of the formalism developed for modeling ${}^7\text{Li} + p \rightarrow {}^8\text{Be} + \gamma$ (or $e^+ + e^-$) in Ref. [9] is that the effects of non-resonant γ production via an $E1$ electric dipole operator is included along with a magnetic dipole $M1$ induced production that goes through intermediate excited states (${}^8\text{Be}^*$). After that, the isospin-rotation relation between Eq. (2) and Eq. (5) will be exploited to compute X -production cross sections.

The photon-production matrix element of the J_γ^μ operator between the initial p - ${}^7\text{Li}(\frac{3}{2}^-)$ system and the ${}^8\text{Be}(0^+)$ ground state is given by $\langle {}^8\text{Be}; -\mathbf{q} | J_\gamma^\mu(\mathbf{q}) | {}^7\text{Li} + p; a, \sigma, \mathbf{p} \rangle$, with a and σ as ${}^7\text{Li}$ and proton spin projections and \mathbf{q} as the (virtual) photon momentum. (From now on, the physical variables in bold fonts, such as \mathbf{q} denote 3-dimensional vectors.) This matrix element has

	$E_{(i)}$ (MeV)	$\Gamma_{\gamma(i)}$ (eV)	$\Gamma_{(i)}$ (keV)
$i = 0$	0.895	$1.9(\pm 0.4)$	$138(\pm 6)$
$i = 1$	0.385	$15.0(\pm 1.8)$	$10.7(\pm 0.6)$

TABLE I. From the left to right: the approximate isospin (i), excitation energies, EM and strong decay widths of the ${}^8\text{Be}$'s two 1^+ resonances [2].

various components, labeled by $U_{\lambda SL}$ [9], with λ , S , and L labeling the γ 's multipolarity (λ), the total spin (S) and orbital angular momentum (L) in the initial state.

The γ production proceeds by either direct proton capture on ${}^7\text{Li}$ (see the right diagram in Fig. 2) or by populating the two intermediate 1^+ excited states [2, 10] of ${}^8\text{Be}$ at relevant beam energies (see the left diagram in Fig. 2). [The properties of the two 1^+ resonances can be found in Fig. 1 and Table. I.] Since the scattering energy between p and ${}^7\text{Li}$ considered here is very low, only s and p waves ($L = 0, 1$) need to be considered in the initial states, while its total spin $S = 1, 2$. Parity and angular momentum conservation leads to selection rules that require only three amplitudes: U_{110} for $E1$, U_{111} and U_{121} for $M1$. The role of the $E2$ transition is negligible [9] and ignored here.

Before discussing the formalism [9] which uses ${}^7\text{Li}$ and p as fundamental degrees of freedom, it is worth understanding the isospin structure of the $U_{\lambda SL}$ on the nucleon level. It provides the key relationship between γ and X production amplitudes.

The single-nucleon electric and magnetic multipole operators are well-known (e.g., see Eqs. (5.45) and (5.71) in Ref. [11]¹). The $E1$ operator is given by

$$\mathcal{O}_{E1}^\gamma = e_{\text{EM}} \sqrt{\frac{3}{4\pi}} \sum_{i=1}^A \mathbf{r}_{(i)} \frac{\tau_{(i),3}}{2}. \quad (6)$$

The summation index (i) labels the nucleons inside ${}^8\text{Be}$ system. The operator \mathcal{O}_{E1}^γ is explicitly isovector. The $M1$ transitions are governed by the operator

$$\begin{aligned} \mathcal{O}_{M1}^\gamma &= \sqrt{\frac{3}{4\pi}} \frac{e_{\text{EM}}}{2M_N} \sum_i \left[\left(\lambda^{(1)} + \frac{1}{4} \right) \boldsymbol{\sigma}_{(i)} \tau_{(i),3} \right. \\ &\quad \left. + \left(\lambda^{(0)} + \frac{1}{4} \right) \boldsymbol{\sigma}_{(i)} + \frac{1}{2} \mathbf{J}_{(i)} (1 + \tau_{(i),3}) \right] \\ &\stackrel{\text{here}}{\approx} \sqrt{\frac{3}{4\pi}} \frac{e_{\text{EM}}}{2M_N} \sum_i \left[\left(\lambda^{(1)} + \frac{1}{4} \right) \boldsymbol{\sigma}_{(i)} + \frac{1}{2} \mathbf{J}_{(i)} \right] \tau_{(i),3} \end{aligned} \quad (7)$$

\mathcal{O}_{M1} is simplified in Eq. (7) based on that (1) the matrix element of the total angular momentum $\mathbf{J} = \sum_i \mathbf{J}_{(i)}$ (assuming the nucleus is made only of nucleons) between

¹ Note the convention of nucleon isospin multiplet in Ref. [11] is $N = (n, p)^T$, which is different from ours in Eq. (2).

the initial resonances and the final state are zero, because \mathbf{J} does not connect states with different angular momentum; and (2) numerically $|\lambda^{(1)} + \frac{1}{4}| (= 2.10) \gg |\lambda^{(0)} + \frac{1}{4}| (= 0.19)$. These expressions for \mathcal{O}_{E1} and \mathcal{O}_{M1} are corrected by two-body meson exchange currents that are mainly transverse and isovector [11, 12]. Therefore both $E1$ and $M1$ transitions here are isovector in nature².

The resulting $E1^X$ and $M1^X$ transition operators for the X production are obtained using Eq. (4) as:

$$\mathcal{O}_{E1}^X = -\varepsilon_v \mathcal{O}_{E1}^\gamma \quad (8)$$

$$\begin{aligned} \mathcal{O}_{M1}^X &= \sqrt{\frac{3}{4\pi}} \frac{e_{EM}}{2M_N} \sum_i \left[-\varepsilon_v \left(\lambda^{(1)} + \frac{1}{4} \right) \boldsymbol{\sigma}_{(i)} \tau_{(i),3} \right. \\ &\quad \left. + \varepsilon_s \left(\lambda^{(0)} + \frac{1}{4} \right) \boldsymbol{\sigma}_{(i)} + \frac{1}{2} \mathbf{J}_{(i)} (\varepsilon_s - \varepsilon_v \tau_{(i),3}) \right] \\ &= \sqrt{\frac{3}{4\pi}} \frac{e_{EM}}{2M_N} \sum_i \left\{ \varepsilon_s \left(\lambda^{(0)} + \frac{1}{4} \right) \boldsymbol{\sigma}_{(i)} \right. \\ &\quad \left. - \varepsilon_v \tau_{(i),3} \left[\left(\lambda^{(1)} + \frac{1}{4} \right) \boldsymbol{\sigma}_{(i)} + \frac{1}{2} \mathbf{J}_{(i)} \right] \right\} \quad (9) \end{aligned}$$

$$\approx -\varepsilon_v \mathcal{O}_{M1}^\gamma \quad (10)$$

The approximation in Eq. (10) would only fail if the isoscalar piece in \mathcal{O}_{M1}^X is not much smaller than the isovector piece in size, i.e.,

$$\left| \frac{\varepsilon_s}{\varepsilon_v} \right| \gtrsim \left| \frac{\lambda^{(1)} + \frac{1}{2}}{\lambda^{(0)} + \frac{1}{4}} \right| \approx 12. \quad (11)$$

In deriving Eq. (9) the spin part of the $\sum_i \tau_{(i),3} \mathbf{J}_{(i)}$ [= $\sum_i \tau_{(i),3} (\mathbf{L}_{(i)} + \boldsymbol{\sigma}_{(i)}/2)$] piece was combined with the $\sum_i \tau_{(i),3} \boldsymbol{\sigma}_{(i)}$ piece; the $\mathbf{L}_{(i)}$ part in the former piece is neglected, because here $\mathbf{L}_{(i)}$ is either 0 or 1 according to shell model and thus its contribution is much smaller than that of $\boldsymbol{\sigma}_{(i)}$.

Accepting the condition of Eq. (11) would require X -proton and -neutron to have almost the same coupling strength, which contradicts X being protophobic. Moreover, including the two-body current contribution to \mathcal{O}_{M1}^X would further increase [12] the dominance of the isovector component over the isoscalar one, and thus makes Eq. (10) a better approximation.

In summary, the $E1^X$ and $M1^X$ operators for protophobic X boson production are (to an excellent approximation) simply proportional to those for the γ production, with an overall factor $-\varepsilon_v$.

Next we briefly describe our effective field theory (EFT) inspired model [9] for γ production, which provides a good description of the cross section data [13], and the space anisotropy data [14, 15]. The model uses ${}^7\text{Li}$ and p as fundamental degrees of freedom to construct the appropriate Lagrangian, so that the model reproduces

the properties of nuclear resonances near ${}^7\text{Li}$ - p threshold, including both MIS and MIV states. Appropriate EM transition vertices are then constructed to describe both direct EM capture process and the radioactive decay of resonant states populated by ${}^7\text{Li}$ - p scattering. Their Feynman diagrams can be found in Fig. 2. The former has smooth dependence on the beam energy while the latter shows resonant behavior. Both components can be qualitatively identified in the γ production data, as shown in the top panel (purple error bars) in Fig. 3.

The next step is to separate the $E1$ and $M1$ contributions to the γ -production cross section and then use the relations in Eqs. (8) and (10) to obtain the $E1^X$ and $M1^X$ contributions to the X -boson production. One may immediately expect that the $E1^X$ contributions will be substantial if the $E1$ and $M1$ contributions are comparable. This is important because the observed enhancement of e^+e^- -pair-production is associated only with an $M1^X$ transition.

The differential cross section can then be computed [9] by using

$$\frac{d\sigma_{\gamma,X}}{d\cos\theta} = \frac{M}{4\pi} \frac{q}{p} \frac{1}{8} \sum_{a,\sigma,\tilde{\lambda}} |\mathcal{M}_{\gamma,X}|^2. \quad (12)$$

Here M is reduced mass between ${}^7\text{Li}$ and proton; θ is the angle between boson momentum \mathbf{q} and beam direction in the CM frame; $q \equiv |\mathbf{q}|$; $p \equiv \sqrt{2ME}$ (E as the CM initial-state kinetic energy with $E = 7/8 E_{\text{lab}}^p$). For both productions, the boson energy $\omega \equiv q^0 = E + E_{\text{th}}$ (E_{th} as the ${}^7\text{Li}$ - p threshold energy wrt the ${}^8\text{Be}$ ground state, see Fig. 1), ignoring the final state ${}^8\text{Be}$'s very small recoiling energy. Note for γ , $\omega = q$, while for X , $\omega = \sqrt{M_X^2 + q^2}$.

The X boson has different polarization-vector structure than the photon. Here we follow Ref. [6], $\partial_\mu X^\mu = 0$, i.e., $q_\mu \varepsilon^\mu(q, \tilde{\lambda}) = 0$ with $\tilde{\lambda}$ as polarization and $\varepsilon^\mu(q, \tilde{\lambda})$ as the corresponding polarization vector. So we have $\sum_{\tilde{\lambda}} \varepsilon^\mu \varepsilon^\nu = -\left(g^{\mu\nu} - \frac{q^\mu q^\nu}{M_X^2}\right)$. The total squared transition amplitudes for the X production, resulting from summing up spin indices and $\tilde{\lambda}$, can be written as

$$\sum_{a,\sigma,\tilde{\lambda}} |\mathcal{M}_X|^2 = \sum_{a\sigma} J_{X,i} J_{X,j}^* \left(\delta_j^i - \frac{q_j q^i}{\omega^2} \right), \quad (13)$$

where \mathbf{J}_X now represents the matrix element of the current operator in Eq. (5), and q_i as the components of \mathbf{q} . This equation is obtained using current conservation for which $J_X^0 J_X^0 = (\mathbf{q} \cdot \mathbf{J}_X)^2 / \omega^2$. For an on-shell photon, $\omega = q$, so the above formula also applies for $\sum_{a,\sigma,\tilde{\lambda}} |\mathcal{M}_\gamma|^2$ with the current changed to \mathbf{J}_γ .

The net result, including only $E1$, $M1$, $E1^X$, and $M1^X$ transitions and evaluating the spin sums, is to arrive at the following decomposition:

$$\sum_{a,\sigma,\tilde{\lambda}} |\mathcal{M}_{\gamma,X}|^2 = T_0^{\gamma,X} + T_1^{\gamma,X} P_1(\cos\theta) + T_2^{\gamma,X} P_2(\cos\theta), \quad (14)$$

² The $M1$ transition has been carefully examined in Ref. [5] which also concludes that it is dominated by the isovector component.

where, P_n are the Legendre polynomials, and

$$T_0^X/\varepsilon_v^2 = (3\omega^2 - q^2)|U_{110}|^2 + \frac{2}{3}q^2 \left(\frac{p}{M}\right)^2 \left[|U_{111}|^2 + |U_{121}|^2\right], \quad (15)$$

$$T_1^X/\varepsilon_v^2 = 2\sqrt{2}\omega q \left(\frac{p}{M}\right) \text{Im}(U_{111}U_{110}^*), \quad (16)$$

$$T_2^X/\varepsilon_v^2 = \frac{1}{3}q^2 \left(\frac{p}{M}\right)^2 \left[|U_{111}|^2 - \frac{1}{5}|U_{121}|^2\right]. \quad (17)$$

Expressions for T_n^γ (that agree with those in Ref. [9]) are obtained from the above formula by using $q = \omega$ and setting ε_v to unity.

Expressions for $U_{\lambda SL}$ in terms of EFT coupling parameters can be found in Ref. [9] in which the model parameters are determined by reproducing the photon production data, including total cross section, T_1^γ/T_0^γ , and T_2^γ/T_0^γ ratios, with the lab energy $E_{\text{lab}}^p \equiv 8/7E$ below 1.5 MeV.

Given these expressions, we turn to the results, starting with the γ -production cross section shown in the upper panel of Fig. 3. The model provides good agreement with the data from Ref. [13]. For further comparisons between theory and experiment see Ref. [9]. The salient features are the two $M1$ resonance contributions, with the lower-energy MIV peak being much higher, and the smooth behavior of those of the $E1$. Except for the strong peaks at the two 1^+ resonances, the $E1$ contributions are dominant.

The resonance peaks occur from a two-step process in which the strong interaction connects the initial $|^7\text{Li}, p\rangle$ to the 1^+ states which then decay by emitting a photon (see the left diagram in Fig. 2). The relative strengths of the two peaks naturally arise from Eq. (7). If the 1^+ states were pure isospin eigenstates, the \mathcal{O}_{M1} operator would only connect the lower-energy state with the ground state. γ -production at the higher-energy resonance occurs only because isospin mixing between the two 1^+ states causes the higher-energy state to have an isospin 1 amplitude of -0.21 [12, 16]. The kinematics together with this ratio can qualitatively explain the photon width comparison $\Gamma_{\gamma(i)}$ shown in Table I [5]. The difference between the strong decay widths shown in that table arises from phase space factors and the greater importance of the Coulomb barrier at lower energies [9]. The final $|^7\text{Li}, p\rangle$ states in the resonances' strong decays are equal mixtures of isospin 0 and 1, so the isospin content of the 1^+ states does not dictate the strong decay width.

Next turn to X production. The total cross section is determined by T_0^X of Eq. (15). The first term of that equation gives the $E1^X$ contribution, and the second gives that of $M1^X$. The $E1^X$ contribution is proportional to $3\omega^2 - q^2$, reflecting the three degrees of freedom for the X boson. For the photon this factor is $2\omega^2$. The q^2 factor in the $M1^X$ contribution arises from the basic magnetic nature of the interaction.

The amplitudes $U_{\lambda SL}$ depend only on the beam energy, E , but not on ω or q [9]. By using $U_{\lambda SL}$ from Ref. [9],

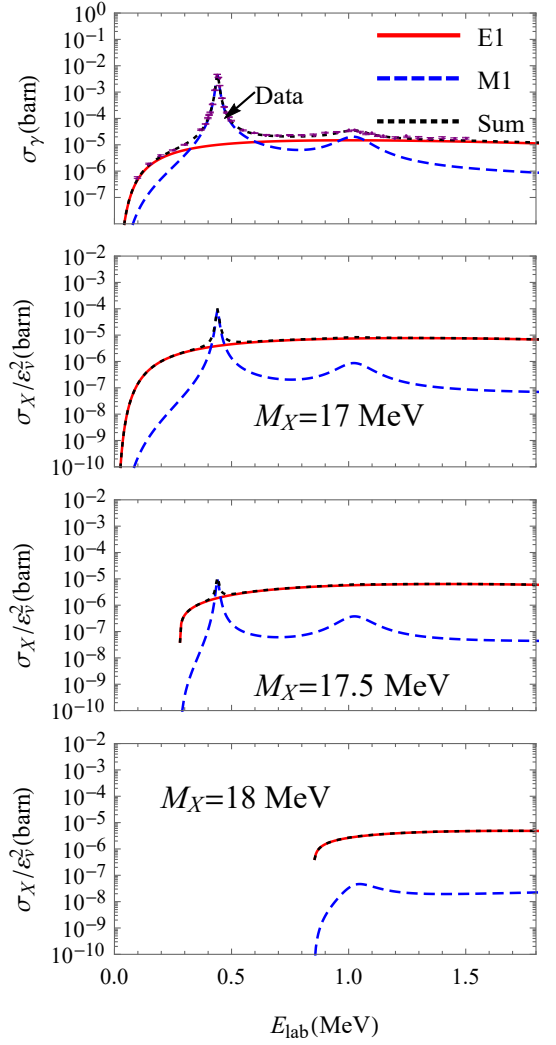


FIG. 3. Top panel: the photon production cross section *vs.* the proton's lab energy E_{lab} . The data are from Ref. [13]. $E1$, $M1$, and their sum are shown as solid (red), dashed (blue), and dotted (black) lines. The lower three panels: our prediction of the X boson production cross sections (scaled by ε_v^2) for different values of M_X . The legends are the same as that in the top panel.

Eq. (15) can be directly used to compute the relative magnitude of the total X production cross section i.e., σ_X/ε_v^2 and its decomposition into the $E1^X$ and $M1^X$ components.

The results thus obtained for three different M_X values (17, 17.5, 18 MeV) around the suggested values from Ref. [3] are shown in the lower three panels of Fig. 3. The X can be produced via the dominant $E1^X$ component for almost *any* energy above the kinematic threshold, except around the MIV resonance for $M_X = 17$ and 17.5 MeV. (Note: the $^7\text{Li}-p$ threshold is 17.26 MeV above ^8Be 's ground state, and thus no kinetic threshold exists for $M_X = 17$ and 17.5 MeV, while such threshold for $M_X = 18$ MeV eliminates X production around the MIV resonance.) This smooth behavior is in direct conflict

with the experimental observation of the pair-production enhancement associated only with the higher energy 1^+ state, if the enhancement is due to X production and its subsequent decay to e^+e^- .

The dominance of the $E1^X$ component around the MIS resonance and the strong dependence of the $E1^X/M1^X$ ratio on the value of M_X , as shown in the figure can be understood using a simple calculation. The ratio can be inferred from the same ratio for the γ production (the phase space factors canceled in the ratios). At a given beam energy E ,

$$\frac{\sigma_{X,E1}(E)}{\sigma_{X,M1}(E)} = \frac{\sigma_{\gamma,E1}(E)}{\sigma_{\gamma,M1}(E)} \frac{3\omega^2 - q^2}{2q^2}, \quad (18)$$

with ω as energy for both X and photon, with $q = \sqrt{\omega^2 - M_X^2}$. Now, at the energy of the MIS resonance where the anomaly was observed, Fig. 3 shows $\sigma_{\gamma,E1} \approx 0.7 \sigma_{\gamma,M1}$. Here $\omega = 18.15$ MeV, and $q = 6.36$ MeV for $M_X = 17$ MeV. Then Eq. (18) tells us that

$$\left. \frac{\sigma_{X,E1}}{\sigma_{X,M1}} \right|_{MIS} = \frac{2\omega^2 + M_X^2}{2(\omega^2 - M_X^2)} \left. \frac{\sigma_{\gamma,E1}}{\sigma_{\gamma,M1}} \right|_{MIS} \stackrel{M_X=17}{\approx} 8.6. \quad (19)$$

The sensitivity to the value of M_X can be seen from the denominator— M_X is close to ω .

The ratio 8.6 is obtained by assuming that Eq. (10) is exact. However to evade this conclusion, $|\varepsilon_s/\varepsilon_v|$ must be

around or larger than 12 as shown in Eq. (11), forcing X to be *protophilic*.

In summary, the results presented in Fig. 3 show that there would be a signal of X production due to $E1^X$ transitions, i.e., Bremsstrahlung radiation of X boson at all beam energies above threshold. This mechanism has a smooth beam energy E dependence, while the resonant production diminishes quickly when E is a few widths away from the resonances. In fact, given a 17 MeV X boson, the enhancement signal should have been seen at *all* four of energies of the ATOMKI experiment [1]. For a 18 MeV X boson, although X production around the MIV resonance is eliminated due to kinematic threshold, the smooth $E1^X$ component should still be detectable above the MIS resonance. However, the experimental observation [1] of the anomaly is absent below or above the MIS, higher-energy 1^+ , resonance. *Therefore, the explanation of the anomaly in terms of protophobic vector boson X cannot be correct.*

ACKNOWLEDGMENTS

X.Z. was supported in part by the National Science Foundation under Grant No. PHY-1913069 and the CSSI program under award number OAC-2004601 (BAND Collaboration), and by the NUCLEI SciDAC Collaboration under Department of Energy MSU subcontract RC107839-OSU. G.M. was supported by the US Department of Energy under contract DE-FG02-97ER-41014. G.M. thanks T. E. O. Ericson for useful discussions.

-
- [1] A. J. Krasznahorkay *et al.*, Phys. Rev. Lett. **116**, no. 4, 042501 (2016).
[2] D. R. Tilley, J. H. Kelley, J. L. Godwin, D. J. Millener, J. E. Purcell, C. G. Sheu and H. R. Weller, Nucl. Phys. A **745**, 155 (2004).
[3] J. L. Feng, B. Fornal, I. Galon, S. Gardner, J. Smolinsky, T. M. P. Tait and P. Tanedo, Phys. Rev. Lett. **117**, no. 7, 071803 (2016);
[4] B. Fornal, Int. J. Mod. Phys. A **32**, 1730020 (2017) doi:10.1142/S0217751X17300204; L. B. Jia and X. Q. Li, Eur. Phys. J. C **76**, no. 12, 706 (2016); U. Ellwanger and S. Moretti, JHEP **1611**, 039 (2016); C. S. Chen, G. L. Lin, Y. H. Lin and F. Xu, Int. J. Mod. Phys. A **32**, no.31, 1750178 (2017); M. J. Neves and J. A. Helayl-Neto, arXiv:1611.07974 [hep-ph]; J. Kozaczuk, D. E. Morrissey and S. R. Stroberg, Phys. Rev. D **95**, no.11, 115024 (2017); P. H. Gu and X. G. He, Nucl. Phys. B **919**, 209-217 (2017) doi:10.1016/j.nuclphysb.2017.03.023; Y. Liang, L. B. Chen and C. F. Qiao, Chin. Phys. C **41**, no.6, 063105 (2017) doi:10.1088/1674-1137/41/6/063105; T. Kitahara and Y. Yamamoto, Phys. Rev. D **95**, no.1, 015008 (2017) doi:10.1103/PhysRevD.95.015008; Y. Kahn, G. Krnjaic, S. Mishra-Sharma and T. M. P. Tait, JHEP **05**, 002 (2017) doi:10.1007/JHEP05(2017)002; O. Seto and T. Shimomura, Phys. Rev. D **95**, no.9, 095032 (2017) doi:10.1103/PhysRevD.95.095032; P. Fayet, Eur. Phys. J. C **77**, no.1, 53 (2017) doi:10.1140/epjc/s10052-016-4568-9; N. V. Krasnikov, arXiv:1702.04596 [hep-ph]; L. Delle Rose, S. Khalil and S. Moretti, Phys. Rev. D **96**, no.11, 115024 (2017) doi:10.1103/PhysRevD.96.115024; D. S. M. Alves and N. Weiner, JHEP **07**, 092 (2018) doi:10.1007/JHEP07(2018)092; L. Delle Rose, S. Khalil, S. King, J.D., S. Moretti and A. M. Thabt, Phys. Rev. D **99**, no.5, 055022 (2019) doi:10.1103/PhysRevD.99.055022; C. Y. Chen, D. McKeen and M. Pospelov, Phys. Rev. D **100**, no.9, 095008 (2019) doi:10.1103/PhysRevD.100.095008; C. H. Nam, Eur. Phys. J. C **80**, no.3, 231 (2020) doi:10.1140/epjc/s10052-020-7794-0; C. Hati, J. Kriewald, J. Orloff and A. M. Teixeira, JHEP **07**, 235 (2020) doi:10.1007/JHEP07(2020)235.
[5] J. L. Feng, B. Fornal, I. Galon, S. Gardner, J. Smolinsky, T. M. P. Tait and P. Tanedo, Phys. Rev. D **95**, no.3, 035017 (2017) doi:10.1103/PhysRevD.95.035017 [arXiv:1608.03591 [hep-ph]].
[6] J. L. Feng, T. Tait, M.P. and C. B. Verhaaren, Phys. Rev. D **102**, no.3, 036016 (2020) doi:10.1103/PhysRevD.102.036016 [arXiv:2006.01151

- [hep-ph]].
- [7] F. Halzen and A. D. Martin, *Quarks and Leptones: An Introductory Course in Modern Particle Physics*, John Willey & Sons (New York), 1984
 - [8] X. Zhang, K. M. Nollett and D. R. Phillips, Phys. Lett. B **751**, 535 (2015); EPJ Web Conf. **113**, 06001 (2016); Phys. Rev. C **89**, no. 5, 051602 (2014); Phys. Rev. C **89**, no. 2, 024613 (2014) .
 - [9] X. Zhang and G. A. Miller, Phys. Lett. B **773**, 159-165 (2017) doi:10.1016/j.physletb.2017.08.013 [arXiv:1703.04588 [nucl-th]].
 - [10] D. R. Tilley, C. M. Cheves, J. L. Godwin, G. M. Hale, H. M. Hofmann, J. H. Kelley, C. G. Sheu and H. R. Weller, Nucl. Phys. A **708**, 3 (2002).
 - [11] R. D. Lawson, *Theory of The Nuclear Shell Model*, (1980) Oxford University Press .
 - [12] S. Pastore, R. B. Wiringa, S. C. Pieper and R. Schiavilla, Phys. Rev. C **90**, no. 2, 024321 (2014)
 - [13] D. Zahnow, C. Angulo, C. Rolfs, S. Schmidt, W. H. Schulte, and E. Somorjai, Z. Phys. A **351**, 229 (1995) .
 - [14] D. J. Schlueter, R. W. Krone, and F. W. Prosser, Nucl. Phys. **58**, 254 (1964) .
 - [15] B. Mainsbridge, Nucl. Phys. **21**, 1 (1960) .
 - [16] R. B. Wiringa, S. Pastore, S. C. Pieper and G. A. Miller, Phys. Rev. C **88**, no. 4, 044333 (2013)